A New Model for Scattering From Tree Canopies Based on Physical Optics and Multiple Scattering Theory

Milan Kvicera, Fernando Pérez Fontán, Jonathan Israel, Pavel Pechac

A New Model for Scattering From Tree Canopies Based on Physical Optics and Multiple Scattering Theory

Milan Kvicera, Fernando Pérez Fontán, Jonathan Israel, and Pavel Pechac, *Senior Member, IEEE*

***Abstract*— This paper presents a new model for scattering from tree canopies based on a modified physical optics approach. In this way, propagation through a canopy is accounted for by respecting the complex propagation constant, which can be obtained either by the multiple scattering theory (MST) or approximated based on the canopy specific attenuation. Unlike the case when MST is applied directly, the proposed approach offers significant benefits, including a straightforward software implementation, feasible computation times for high frequencies and electrically large canopies, and, most importantly, near-field calculations in regions close to a canopy. The new model is first tested against MST using two artificial single-tree scenarios at 2 and 10 GHz. Then, experimental data at 2 GHz obtained with the use of a remote controlled airship for an actual single-tree scenario are utilized as well. In this way, the model is thoroughly validated and its advantages over MST are presented in detail.**

***Index Terms*— Multiple scattering theory (MST), physical optics (PO), scattering, vegetation.**

I. Introduction

SCATTERING from tree canopies has always been of great interest when addressing radio-wave propagation in the presence of vegetation. This results in different methods given in the corresponding Recommendation ITU-R P.833-8 [1] distinguishing the case of a woodland and an isolated tree. For example, in woodlands, it is only necessary to consider specific attenuation in dB/m at the frequency of interest and obtain the resulting signal attenuation based on the path length through the vegetation. Such straightforward approach cannot be applied for a scenario with a single isolated tree. Thus, in addition to diffraction around a canopy and a ground reflection, [1] utilizes the theory of radiative energy transfer for propagation through the canopy.

However, the above-mentioned model for isolated trees is applicable only when the direction from a transmitter (Tx) toward the canopy is the same as from the canopy toward a receiver (Rx), which is generally not the case. Lately, a slant path scenario based on the multiple scattering theory (MST) has been added to [1] to overcome such limitations.

MST as given in [1] is based on [2] and [3], which, in turn, utilize mainly [4] and [5]. It should be noted that the theoretical background of MST applicable to electromagnetic wave propagation was first given by [6]–[8] and also utilized in [9] and [10] for the case of a plane wave incident obliquely on a tree canopy represented by a slab of leaves and branches.

With the advent of communication and navigation wireless services, there is an increasing demand on them to reliably operate outdoors also in the presence of vegetation. This requirement calls for a model enabling a proper characterization of such environments in a site-specific way, respecting different types and sizes of trees together with various incoming and outgoing propagation directions.

So far, this resulted, for example, in the characterization of a single-tree scattering pattern by means of computationally demanding finite-difference time domain [11], canopy volume being filled with point source scatterers [12] or [13], high-frequency measurement campaigns [14], or measurements of specific attenuation for different types of trees or seasons [15]–[17].

Following [1], site-specific characterization of tree scattering can be nicely satisfied by utilizing MST as its input values include, among others, thorough physical characteristics, such as sizes of branches and leaves together with their electrical parameters, number densities, and spatial orientation statistics.

However, there are two main drawbacks of MST preventing its widespread usage. The first is its complexity resulting in a nontrivial implementation as a computer program, even when [1] is followed step by step. The second is the enormous computation time required caused by summation of the high-order Hankel and Bessel functions and canopy volume integration, as denoted in [3] and [18].

In general, MST provides two types of scattered fields, coherent and incoherent [4]. As shown in [3] and [18], in other than the forward scatter direction, the incoherent field may dominate in amplitude. On the other hand, shadowing behind a canopy results from the coherent field [3], which is, thus, of interest in [1] as well as in this paper.

As far as shadowing behind a canopy is considered, physical optics (PO) [19], [20], as applied in [21], offers a computationally very efficient way to calculate the coherent scattered field behind an electrically large dielectric object, but it excludes

any field passing through it. However, in the following, we present how to overcome this limitation by considering a complex propagation constant within the canopy, similar to the approach carried out in [9] and implemented in [10]. In this way, it is possible to replace MST by PO and obtain a significantly less computationally demanding model with a straightforward software implementation. Following the PO approach of [9], the present approach includes the equivalent electric and magnetic currents on the inner surface of a tree canopy, which acts as a radiating aperture allowing to account for diffraction effects around the canopy.

Other significant advantages of such model include a proper modeling of near-field effects close to the canopy and the fact that the consideration of fields going through and around the canopy gives rise to smooth transitions between the shadowed and line of sight (LoS) areas behind the canopy. In contrast, a linear model based only on the specific attenuation inevitably results in sharp edge effects within the transition area where the abrupt change is a consequence of the path through the canopy identified solely in a geometrical manner.

We also show that the presented model provides results in agreement with both MST and experimental data obtained for a single-tree scenario at 2 GHz. It may be also applied to high frequencies or even a group of trees as it requires only sampling of the surface instead of the object's volume, which is the case of MST. Thus, it respects the recent trend of the frequency increase toward Ka-band and above in satellite communication systems where the influence of vegetation must be thoroughly addressed from the radio-wave propagation point of view.

Section II provides a theoretical background for both PO and MST. In Section III, the new combined PO/MST model is introduced. Its validation against MST and experimental data set is presented in Sections IV and V, respectively. Section VI concludes this paper.

II. Theoretical Background

A. Physical Optics

Following [19] and [20], both the electric $\mathbf{J}_{\text{eq}}$ and magnetic $\mathbf{M}_{\text{eq}}$ equivalent surface currents are considered for the time-harmonic case enabling to drop the $e^{j\omega t}$ time dependence. In addition, only an incident plane wave in free space is assumed, and thus, the electric field incident on an object's surface sample can be written as

$$\mathbf{E}_{\text{inc}} = E_0 \mathrm{e}^{-j\mathbf{k}\cdot\mathbf{r}} \tag{1}$$

where E_0 is the amplitude in V/m, $\mathbf{r}$ is the surface sample positioning vector, and

$$\mathbf{k} = k_0 \hat{\mathbf{k}}_{\text{inc}} \tag{2}$$

where k_0 is the free space wavenumber and $\hat{\mathbf{k}}_{\text{inc}}$ is the unitary vector in the plane wave incident direction.

The incident magnetic field is related to $\mathbf{E}_{\text{inc}}$ by [19]

$$\mathbf{H}_{\text{inc}} = (1/Z_0)\hat{\mathbf{k}}_{\text{inc}} \times \mathbf{E}_{\text{inc}} \tag{3}$$

where Z_0 is the characteristic impedance of free space.

For a perfectly absorbing object, there are no reflected fields on the object's surface, and, based on the boundary conditions

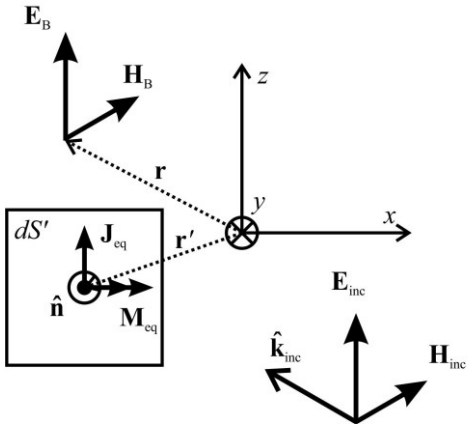

Fig. 1. Illustration of the incident fields $\mathbf{E}_{\text{inc}}$ and $\mathbf{H}_{\text{inc}}$, the electric $\mathbf{J}_{\text{eq}}$ (single arrow), and magnetic $\mathbf{M}_{\text{eq}}$ (double arrow) equivalent currents on a totally absorbing surface sample of area dS at $\mathbf{r}$ and the resulting fields $\mathbf{E}_B$ and $\mathbf{H}_B$ at $\mathbf{r}$ considering a rectangular xyz coordinate system. Normal vector $\hat{\mathbf{n}}$ of the surface sample is pointing outward in the $-y$-direction.

for tangential electric and magnetic fields, the following relations apply [19], [20]:

$$\mathbf{M}_{\text{eq}} = -\hat{\mathbf{n}} \times \mathbf{E}_{\text{inc}} \tag{4}$$

$$\mathbf{J}_{\text{eq}} = \hat{\mathbf{n}} \times \mathbf{H}_{\text{inc}} \tag{5}$$

where $\hat{\mathbf{n}}$ is the unit normal vector of the surface sample at $\mathbf{r}$ pointing outward. In this case, the surface samples illuminated by the incident plane wave satisfy $\hat{\mathbf{k}}_{\text{inc}} \cdot \hat{\mathbf{n}} < 0$.

By using $\mathbf{M}_{\text{eq}}$ and $\mathbf{J}_{\text{eq}}$, the scattered electric and magnetic near fields at point $\mathbf{r}$ are [19]

$$\mathbf{H}_{\text{scat,J}} = -jk_0 \frac{e^{-jk_0|\mathbf{r}-\mathbf{r}'|}}{4\pi|\mathbf{r}-\mathbf{r}'|} \frac{\mathbf{r}-\mathbf{r}'}{|\mathbf{r}-\mathbf{r}'|} \times \mathbf{J}_{\text{eq}} dS \tag{6}$$

$$\mathbf{E}_{\text{scat,M}} = jk_0 \frac{e^{-jk_0|\mathbf{r}-\mathbf{r}'|}}{4\pi|\mathbf{r}-\mathbf{r}'|} \frac{\mathbf{r}-\mathbf{r}'}{|\mathbf{r}-\mathbf{r}'|} \times \mathbf{M}_{\text{eq}} dS \tag{7}$$

where dS is the area of the corresponding surface sample.

It should be noted that the following relations must be utilized to get the electric field contribution $\mathbf{E}_{\text{scat,J}}$ from $\mathbf{J}_{\text{eq}}$ and the magnetic field contribution $\mathbf{H}_{\text{scat,M}}$ from $\mathbf{M}_{\text{eq}}$:

$$\mathbf{E}_{\text{scat,J}} = -Z_0 \hat{\mathbf{k}} \times \mathbf{H}_{\text{scat,J}} \tag{8}$$

$$\mathbf{H}_{\text{scat,M}} = 1/Z_0 \hat{\mathbf{k}} \times \mathbf{E}_{\text{scat,M}}. \tag{9}$$

As in [19], the scattered fields in (6)–(9) introduce blockage of the original plane wave fields $\mathbf{E}_{\text{dir}}$ and $\mathbf{H}_{\text{dir}}$, which would exist at $\mathbf{r}$ if the object was not present. When added together, the resulting fields in the presence of a perfectly absorbing obstacle are

$$\mathbf{E}_B = \mathbf{E}_{\text{dir}} + (\mathbf{E}_{\text{scat,J}} + \mathbf{E}_{\text{scat,M}}) = \mathbf{E}_{\text{dir}} + \mathbf{E}_{\text{block}} \tag{10}$$

$$\mathbf{H}_B = \mathbf{H}_{\text{dir}} + (\mathbf{H}_{\text{scat,J}} + \mathbf{H}_{\text{scat,M}}) = \mathbf{H}_{\text{dir}} + \mathbf{H}_{\text{block}} \tag{11}$$

creating a diffraction pattern behind the canopy. The whole approach is shown in Fig. 1 in a rectangular xyz coordinate system.

B. Multiple Scattering Theory

As in [1]–[3] and [18], two main simplifying assumptions are required, so that the coherent fields scattered from tree canopies can be calculated by MST. First, all scattering paths, which go through a scatterer more than once, are neglected. Second, the amplitude of the incident plane wave is supposed to be constant over the whole canopy.

Then, the coherent field at $\mathbf{r}$ inside the canopy can be written as [3], [18]

$$\mathbf{E}_{\text{coh}}^{\text{in}}(\mathbf{r}) = \mathbf{E}_{\text{inc}} \exp\{-j(K - k_0)s_1(\mathbf{r})\} \tag{12}$$

where $\mathbf{E}_{\text{inc}}$ is the incident plane wave as in (1), $s_1(\mathbf{r})$ is the distance through the canopy to $\mathbf{r}$ along $\hat{\mathbf{k}}_{\text{inc}}$, and K is the complex propagation constant inside the canopy given in [9] for a slab of scatterers as

$$K = K' - jK'' = k_0 \sin(\theta) + \frac{2\pi}{k_0 \sin(\theta)} F^{\text{eq}}(\hat{\mathbf{k}}_{\text{inc}}, \hat{\mathbf{k}}_{\text{inc}}) \tag{13}$$

with $F^{\text{eq}}(\hat{\mathbf{k}}_{\text{inc}}, \hat{\mathbf{k}}_{\text{inc}})$ representing the canopy's equivalent scattering amplitude per unit volume in the forward scatter direction and the incident slant angle denoted by θ.

The resulting coherent scattered field in $\hat{\mathbf{k}}_{\text{out}}$ direction at $\mathbf{r}$ can now be written as [3], [18]

$$\mathbf{E}_{\text{scat}} = \int_V F^{\text{eq}}(\hat{\mathbf{k}}_{\text{out}}, \hat{\mathbf{k}}_{\text{inc}}) \frac{\exp(-jk_0|\mathbf{r} - \mathbf{r}'|)}{|\mathbf{r} - \mathbf{r}'|} \mathbf{E}_{\text{coh}}^{\text{in}}(\mathbf{r}') \, \mathrm{d}V \tag{14}$$

where $\cdot$ denotes the statistical average and the integration is performed over the whole canopy.

The restriction to 2-D scenarios and cylindrical canopies in [2] and [3] can be overcome by integrating (14) numerically as in [18]. Furthermore, it should be noted that $F^{\text{eq}}(\hat{\mathbf{k}}_{\text{out}}, \hat{\mathbf{k}}_{\text{inc}})$ can be obtained for arbitrary directions and polarizations following [5].

It should be noted that in [9], (13) is obtained from Maxwell's equations by finding the mean field in the canopy to its first order of approximation (for the general case of oblique incidence relative to the canopy). However, considering spherical canopies, it is difficult to uniquely distinguish between the perpendicular and oblique incidence, especially in the case of other than terrestrial links. Thus, the model presented in the following assumes the incidence to be perpendicular for any $\hat{\mathbf{k}}_{\text{inc}}$, i.e., $\theta = 90°$ in (13), and the distances through the canopy toward the illuminated inner surface samples are taken always along $\hat{\mathbf{k}}_{\text{inc}}$. As a consequence, this also allows for considering a plane wave incident directly on the top of a canopy, as is common for satellite services during the overhead passes.

When the scattered field is added to the direct field, as in (10), shadowing behind the canopy is obtained. However, as denoted in [3] and [18], the computational demands become unwieldy with increasing frequency and larger canopies, mainly due to the calculations of $F^{\text{eq}}(\hat{\mathbf{k}}_{\text{out}}, \hat{\mathbf{k}}_{\text{inc}})$ and the numerical integration in (14).

III. New PO/MST Model

In Section II-B, PO for the case of a completely absorbing object was presented. If propagation through a canopy based on K was addressed by PO as well, computationally demanding MST calculations could be avoided. Such modification of PO is introduced as follows. In addition, the possibility to approximate K based on canopy specific attenuation is provided.

A. Modified PO Approach

Based on (10), we may note that it is possible to obtain $\mathbf{E}_{\text{dir}}$ at $\mathbf{r}$, i.e., as if the perfectly absorbing object was not present, by eliminating the blockage field in the following way:

$$\mathbf{E}_{\text{dir}} = \mathbf{E}_{\text{dir}} + \mathbf{E}_{\text{block}} - \mathbf{E}_{\text{block}}. \tag{15}$$

In terms of PO, $-\mathbf{E}_{\text{block}}$ can be obtained as $\mathbf{E}_{\text{block}}$ for $\hat{\mathbf{n}}$ pointing in the opposite direction than in Fig. 1, i.e., as if dS was a radiating aperture instead of a blocking element, thus providing an aperture field $\mathbf{E}_{\text{aper}}$. In fact, this situation follows Babinet's principle in optics [20], which states that the field in case of no screen ($\mathbf{E}_{\text{dir}}$) equals the sum of the field behind a screen with an opening/aperture ($-\mathbf{E}_{\text{block}}$) and the field of the complementary structure ($\mathbf{E}_{\text{block}}$).

This can now be utilized to build a basis of the modified PO model. We keep the field in the presence of the perfectly absorbing obstacle $\mathbf{E}_{\text{B}}$ and $\mathbf{H}_{\text{B}}$ [see (10) and (11)], and adjust the aperture field $\mathbf{E}_{\text{aper}}$ and $\mathbf{H}_{\text{aper}}$ based on the propagation characteristics of the object. The resulting total fields can be written as

$$\mathbf{E}_{\text{tot}} = \mathbf{E}_{\text{B}} + \mathbf{E}_{\text{aper}} = (\mathbf{E}_{\text{dir}} + \mathbf{E}_{\text{block}}) + \mathbf{E}_{\text{aper}} \tag{16}$$

$$\mathbf{H}_{\text{tot}} = \mathbf{H}_{\text{B}} + \mathbf{H}_{\text{aper}} = (\mathbf{H}_{\text{dir}} + \mathbf{H}_{\text{block}}) + \mathbf{H}_{\text{aper}}. \tag{17}$$

For the case of a completely transparent object where $\mathbf{E}_{\text{aper}} = -\mathbf{E}_{\text{block}}$, (16) fulfills that $\mathbf{E}_{\text{tot}}$ must equal $\mathbf{E}_{\text{dir}}$ as

$$\mathbf{E}_{\text{tot}} = (\mathbf{E}_{\text{dir}} + \mathbf{E}_{\text{block}}) - \mathbf{E}_{\text{block}} = \mathbf{E}_{\text{dir}}. \tag{18}$$

However, should the object be less transparent, $\mathbf{E}_{\text{aper}}$ must be accordingly adjusted so that it even vanishes as the object becomes totally absorbing for which, as in (10)

$$\mathbf{E}_{\text{tot}} = (\mathbf{E}_{\text{dir}} + \mathbf{E}_{\text{block}}) + 0 = \mathbf{E}_{\text{B}}. \tag{19}$$

Similar situation applies to the magnetic fields as well.

Now, we can present the resulting model in more detail. Considering a cylindrical canopy, which can also be of any other shape if its surface is sampled properly, the top view of the corresponding scenario is shown in Fig. 2.

Commonly, in PO, the outer surface visible by the incoming plane wave is identified to enable the calculation of the scattered fields. However, it is here more advantageous to consider the inner surface to be illuminated ($\hat{\mathbf{k}}_{\text{inc}} \cdot \hat{\mathbf{n}} > 0$ for $\hat{\mathbf{n}}$ pointing outward the surface, solid line in Fig. 2). The reason is that K can then be applied directly in (1) based on the path through the canopy in $\hat{\mathbf{k}}_{\text{inc}}$ direction toward $\mathbf{r}$ as

$$\mathbf{E}_{\text{inc}} = E_0 \mathrm{e}^{-jk_0 \hat{\mathbf{k}}_{\text{inc}} \cdot \mathbf{r}} \, \mathrm{e}^{-j(K - k_0)s_1(\mathbf{r})} \tag{20}$$

similar to (12). After that, (3)–(9) can be applied directly to obtain

$$\mathbf{E}_{\text{aper}} = \mathbf{E}_{\text{scat,J}} + \mathbf{E}_{\text{scat,M}} \tag{21}$$

$$\mathbf{H}_{\text{aper}} = \mathbf{H}_{\text{scat,J}} + \mathbf{H}_{\text{scat,M}} \tag{22}$$

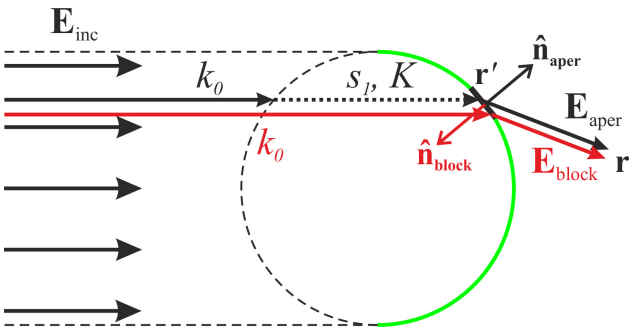

Fig. 2. Modified PO approach illustrated by the top view of a cylindrical canopy illuminated by a plane wave $\mathbf{E}_{\text{inc}}$. The outer part of the canopy visible by $\mathbf{E}_{\text{inc}}$ is shown by the dashed line. However, the model considers the inner part shown by the green solid line to be illuminated by $\mathbf{E}_{\text{inc}}$. The field radiated from the inner aperture toward $\mathbf{r}$, $\mathbf{E}_{\text{aper}}$, is obtained by considering the surface sample normal pointing outward and the complex propagation constant K inside the canopy within the path length s_1. The blockage field, $\mathbf{E}_{\text{block}}$, is obtained by considering the surface sample normal pointing inward and k_0 only.

with $\hat{\mathbf{n}} = \hat{\mathbf{n}}_{\text{aper}}$ oriented as in Fig. 2. This makes the model very straightforward and results in low computational demands. Otherwise, if the outer surface (dashed line in Fig. 2) was considered to be illuminated by $\mathbf{E}_{\text{inc}}$, a unique propagation direction and path lengths through the canopy would have to considered inside (6) and (7) for each $\mathbf{r}$, inappropriately complicating the model.

When compared with [9] or [10], which can be used for the case of a single isolated tree as well, we should stress that (21) and (22) utilize $\mathbf{M}_{\text{eq}}$ and $\mathbf{J}_{\text{eq}}$ induced on the illuminated inner surface of the canopy. Such concept is also compatible with the PO approach of common electromagnetic simulators.

The blockage fields $\mathbf{E}_{\text{block}}$ and $\mathbf{H}_{\text{block}}$ are obtained as in (1)–(10) with $\hat{\mathbf{n}} = \hat{\mathbf{n}}_{\text{block}}$ oriented as in Fig. 2. Direct fields at $\mathbf{r}$ simply follow (1) and (3) as:

$$\mathbf{E}_{\text{inc}} = E_0 \mathrm{e}^{-j\mathbf{k}\cdot\mathbf{r}} \tag{23}$$

$$\mathbf{H}_{\text{inc}} = (1/Z_0)\hat{\mathbf{k}}_{\text{inc}} \times \mathbf{E}_{\text{inc}}. \tag{24}$$

B. Propagation Inside Canopy

Following [3], the field inside the canopy depends on K as:

$$\mathbf{E}(\mathbf{r}) \sim \exp\{-jKs_1(\mathbf{r})\} = \exp\{-j(K - jK)s_1(\mathbf{r})\}. \tag{25}$$

However, in [20], propagation constant γ is considered, such that

$$\mathbf{E}(\mathbf{r}) \sim \exp\{-\gamma s_1(\mathbf{r})\} = \exp\{-(\alpha + j\beta)s_1(\mathbf{r})\} \tag{26}$$

and

$$\gamma = \sqrt{-\omega^2\mu\varepsilon + j\omega\mu\sigma} \tag{27}$$

where ω is the angular frequency and μ, ε, and σ are the permeability, permittivity, and conductivity of the medium, respectively.

This allows us to write

$$\beta = K = Re\{K\} \tag{28}$$

$$\alpha = K = -Im\{K\} \tag{29}$$

and derive relative permittivity ε_r and conductivity σ of the canopy as

$$\varepsilon_r = \frac{\alpha^2 - \beta^2}{-\omega^2\mu_0\varepsilon_0} = \frac{K^2 - K^2}{\omega^2\mu_0\varepsilon_0} \tag{30}$$

$$\sigma = \frac{2\alpha\beta}{\omega\mu_0} = \frac{2K\,K}{\omega\mu_0} \tag{31}$$

where the permittivity and permeability of vacuum are $\varepsilon_0 = 8.854 \times 10^{-12}$ F/m and $\mu_0 = 4\pi \times 10^{-7}$ H/m, respectively.

Based on [3], the specific attenuation in dB/m is then

$$\alpha_{\text{spec}} = 8.686K = 8.686\alpha. \tag{32}$$

It should be noted that K can be well approximated by k_0 as, generally, more volume of the canopy consists of free space rather than branches and leaves. Under this assumption, it is possible to avoid calculations of K by MST if the specific attenuation for a given type of tree is given as, for example, by [1]. Then, we may write

$$K \cong k_0 - jK = k_0 - j\alpha_{\text{spec}}/8.686. \tag{33}$$

This means that if this approximation is used in (20), MST calculations are avoided completely, further reducing the computational time. However, as shown in Section IV, a better agreement with MST is achieved when both the phase and amplitude changes are applied in (20).

We should note that following [9], (13) is valid under the approximation that the total field incident on a scatterer is equal to the mean field, which sets a validity limit on the upper frequency as the path through the canopy should be below one or two skin depths [22]. As the skin depth is the inverse of K [22], we may consider $\alpha_{\text{spec}} = 2$ dB/m at 10 GHz [1], and, with the use of (32), we obtain the skin depth of about 4.3 m. In the same way, at 2 GHz, the skin depth would be about 21.7 m. This justifies the validity of all the simulations presented in this paper.

IV. Validation Against MST

There exist an unlimited number of scenarios to validate the presented model. Following [18], two distinct frequencies, namely, 2 and 10 GHz, are selected to demonstrate the computational advantage of the modified PO model over MST. All the simulation times are related to a PC with a 3.5-GHz Quad-Core processor and 16-GB RAM.

As in [1], both the terrestrial path ($\hat{\mathbf{k}}_{\text{inc1}}$ in Fig. 3) and a slant path ($\hat{\mathbf{k}}_{\text{inc2}}$ in Fig. 3), for which the elevation angle of 20° was selected, are addressed. The canopy of interest is a cylinder of radius $R = 1$m and height $H = 2$m and the incident plane wave is supposed to be vertically polarized. The resulting vertically polarized fields are calculated in two straight lines with a sampling step of one third of the wavelength, $\lambda/3$. The first one is in the x-direction starting from behind the canopy up to a distance of 500λ (see Fig. 3) to simulate a scenario where Rx moves away from the canopy. The second one is 50λ long starting at a distance of 0.5m behind the canopy following the y-direction to present a scenario when Rx moves out of the shadowed area behind the canopy.

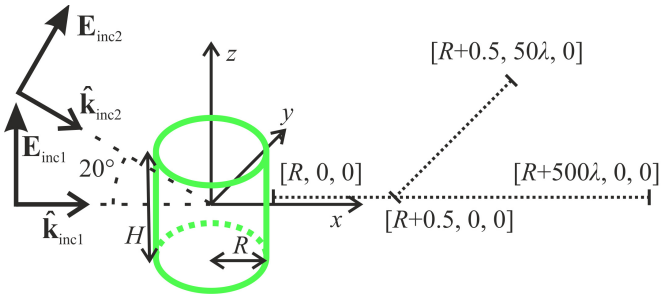

Fig. 3. Validation scenario considering two different incident angles of the incident plane wave (elevation of 0° and 20° with respect to the cylindrical canopy of radius $R = 1$m and height $H = 2$m with a center at the origin of the xyz coordinate system. The resulting fields are obtained behind the canopy in a line from $[R, 0, 0]$ to $[R + 500\lambda, 0, 0]$, i.e., parallel to x, and from $[R + 0.5, 0, 0]$ to $[R + 0.5, 500\lambda, 0]$, i.e., parallel to y, with a sampling step of $\lambda/3$ as indicated by the dotted lines.

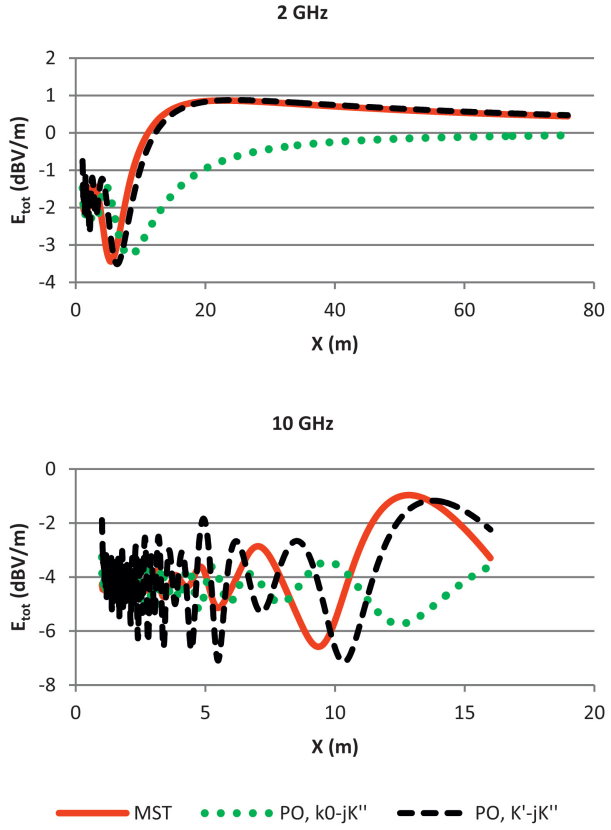

Fig. 4. Total field behind the canopy in the x-direction from R up to $R+500\lambda$ at 2 GHz (top) and 10 GHz (bottom) as obtained by MST (solid line) and the modified PO approach (dashed line) for which the results with approximated $K \cong k_0 - jK$ (dotted line) are shown as well. The incident plane wave with vertical polarization is perpendicular to the canopy.

To avoid any inconsistence with [1]–[3] and [18], the same material parameters, sizes, and orientation of the branches and leaves were considered. As a consequence, the propagation constant obtained by (13) is $K_{2\text{GHz}} = 42.06 - 0.11i$ and $K_{10\text{GHz}} = 210.34 - 0.25i$. In terms of (30) and (31), this implies $\varepsilon_{r,2\text{GHz}} = 1.007$, $\sigma_{2\text{GHz}} = 0.0006$ S/m and $\varepsilon_{r,10\text{GHz}} = 25.18$, $\sigma_{10\text{GHz}} = 0.0067$ S/m. Following (32), the specific attenuation is $\alpha_{\text{spec},2\text{GHz}} = 0.96$ dB/m and $\alpha_{\text{spec},10\text{GHz}} = 2.17$ dB/m.

Based on Fig. 4, which shows the scan in the x-direction for the perpendicular incident plane wave, it is obvious that

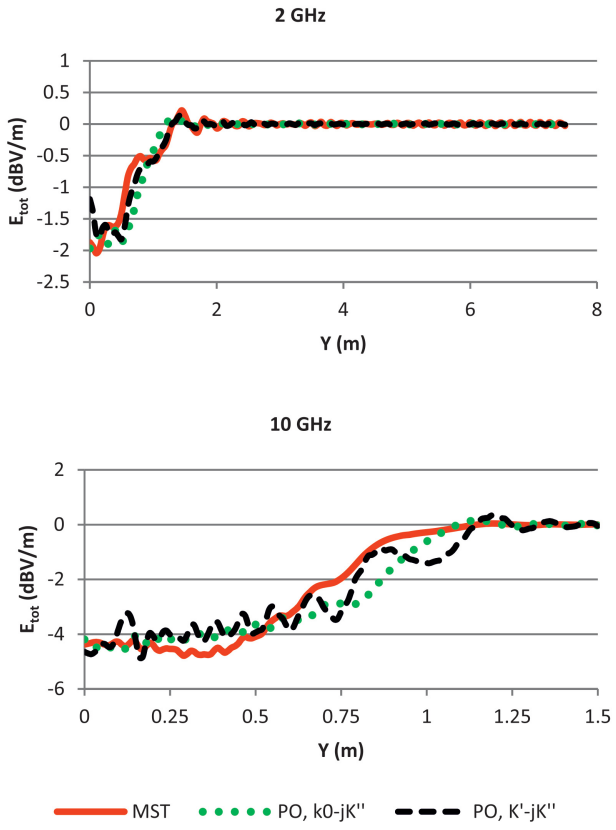

Fig. 5. Total field behind the canopy up to a distance of 50λ in the y-direction for $x = R + 0.5$ at 2 GHz (top) and 10 GHz (bottom) as obtained by MST (solid line) and the modified PO approach (dashed line) for which the results with approximated $K \cong k_0 - jK$ (dotted line) are shown as well. The incident plane wave with vertical polarization is perpendicular to the canopy.

the modified PO approach follows the MST trend in a better way when the approximation of K is not utilized, especially at 2 GHz. This is also the case in Fig. 5, where the scan in the y-direction is shown. With increasing distance, the resulting field is smoothly approaching the incident plane wave field of the amplitude $E_0 = 0$dBV/m in both Figs. 4 and 5. Moreover, we may note that in Fig. 5, as expected, this transition occurs approximately at a distance of 1 m in the y-direction where, based on the canopy radius, the geometrical LoS begins. The overall attenuation behind the canopy is about 2 and 4 dB at 2 and 10 GHz, respectively, which nicely corresponds to the maximum path through the canopy, which is 2 m, multiplied by $\alpha_{\text{spec},2\text{ GHz}}$ or $\alpha_{\text{spec},10\text{ GHz}}$ given earlier.

It must be noted that, for particular $\mathbf{r}$, MST based on (14) considers K being the same for each canopy voxel [3], [18]. This is, however, a far-field approximation considering the scattered fields to be emanating from the canopy's center. Without this consideration, MST would be impossible to run in this case. However, the modified PO approach utilizes near-field propagators (6) and (7) accounting for different directions from each surface sample and is thus capable to adequately represent canopy's near fields. This can be observed in Figs. 4–7 where, close to the canopy, stronger field variations are provided by the modified PO model than by MST. Note that due to the canopy dimensions, results at 10 GHz

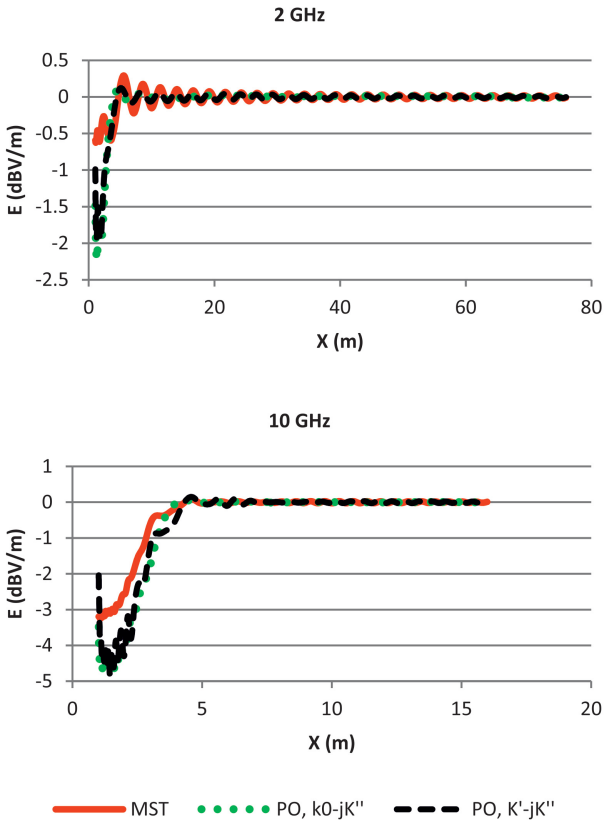

Fig. 6. Total field behind the canopy in the x-direction from R up to $R+500\lambda$ at 2 GHz (top) and 10 GHz (bottom) as obtained by MST (solid line) and the modified PO approach (dashed line) for which the results with approximated $K \cong k_0 - jK$ (dotted line) are shown as well. The incident plane wave with vertical polarization has an elevation angle of 20° with respect to canopy center.

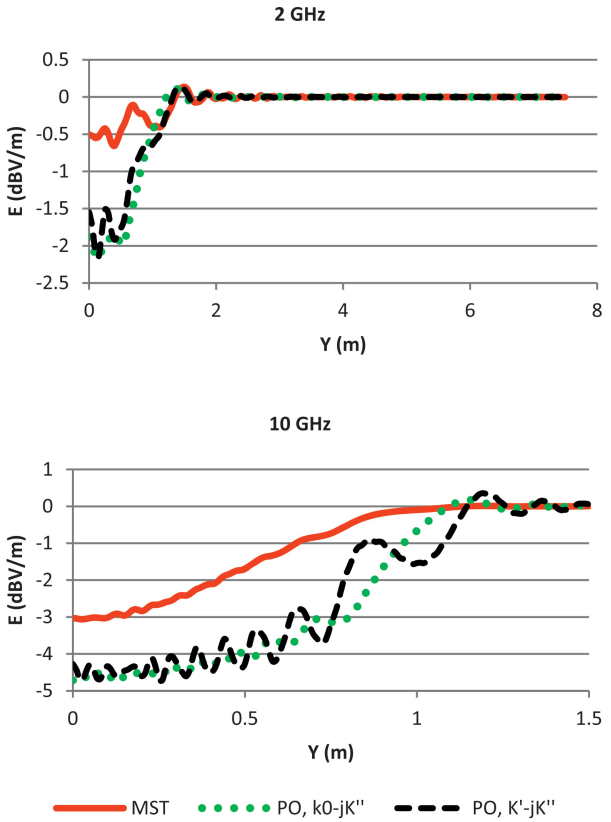

Fig. 7. Total field behind the canopy up to a distance of 50λ in the y direction for $x = R + 0.5$ at 2 GHz (top) and 10 GHz (bottom) as obtained by MST (solid line) and the modified PO approach (dashed line) for which the results with approximated $K \cong k_0 - jK$ (dotted line) are shown as well. The incident plane wave with vertical polarization has an elevation angle of 20° with respect to canopy center.

in Figs. 4 and 5 can be considered as near fields, indicating a limited validity of MST and the worse match with the modified PO model.

Figs. 6 and 7 show the same scenarios as Figs. 4 and 5; however, the incident plane wave has now an elevation angle of 20°. Here, the advantage of not using the approximation of K is not that pronounced, although it still results in more realistic stronger near-field variations.

We should note that, from the geometrical point of view, the influence of $\mathbf{E}_{\text{dir}}$ is stronger than in the case of the perpendicular incidence, and thus, the free space conditions are achieved at shorter distances and the resulting curves are smoother than in Figs. 4 and 5.

Again, similar to Figs. 4 and 5, we see smooth transitions between shadowed and LoS areas respecting the geometrical LoS, which now begins at about 4 m in the x-direction in Fig. 6, based on the elevation angle and canopy height, and remains almost the same in Fig. 7 as in Fig. 5.

Furthermore, apart from the near-field limitations, about 1-dB lower attenuation level predicted by MST in Fig. 6 is a consequence of the fact that the coherent scattered field predicted by MST significantly decreases for other than the forward scatter direction [3], [18]. Thus, for the slant path, MST predicts lower resulting attenuation as $|F^{\text{eq}}(\hat{\mathbf{k}}_{\text{out}}, \hat{\mathbf{k}}_{\text{inc}})| \leq |F^{\text{eq}}(\hat{\mathbf{k}}_{\text{inc}}, \hat{\mathbf{k}}_{\text{inc}})|$ whereas the modified PO model is based solely on the forward scatter case due to using K within the canopy.

PO computation times at 2 and 10 GHz for the scenario in Fig. 4 were 4 s and 1.5 min, respectively, excluding the time needed to sample the canopy by squares of side $\lambda/3$ and obtain K based on (13), which had to be calculated only once as $\hat{\mathbf{k}}_{\text{inc}}$ did not change. MST required 40.2 and 52.7 min to obtain $F^{\text{eq}}(\hat{\mathbf{k}}_{\text{out}}, \hat{\mathbf{k}}_{\text{inc}})$ for each $\mathbf{r}$ at 2 and 10 GHz, respectively, and then 1 s and 3.2 min for the volume integration in (14) where the voxel side was 0.4λ as in [18]. The scenario in Fig. 5 with ten times shorter Rx path required about ten times less computation time, as expected. Similar situation was observed for the scenarios in Figs. 6 and 7 as well.

This allows us to compare computation times per one $\mathbf{r}$ position, as shown in Table I. It turns out that if $F^{\text{eq}}(\hat{\mathbf{k}}_{\text{out}}, \hat{\mathbf{k}}_{\text{inc}})$ was precalculated, as in [2] and [3], the performance of PO and MST would be for this specific case about the same at 2 GHz, with PO becoming faster at 10 GHz, as could be expected. However, using MST would thus mean that only scenarios known in advance can be considered, and, as already discussed, near-field calculations would be disregarded. In addition, for frequencies toward Ka-band and above, the number of voxels for electrically large canopies

TABLE I
COMPUTATION TIMES PER ONE RX POSITION

Method	Time (s)
MST, $F^{eq}(\hat{\mathbf{k}}_{\text{out}}, \hat{\mathbf{k}}_{\text{inc}})$, 2 GHz	1.6
MST, volume integration (14), 2 GHz	0.001
Modified PO, 2 GHz	0.003
MST, $F^{eq}(\hat{\mathbf{k}}_{\text{out}}, \hat{\mathbf{k}}_{\text{inc}})$, 10 GHz	2.1
MST, volume integration (14), 10 GHz	0.13
Modified PO, 10 GHz	0.06

becomes enormous, thus significantly increasing computation demands of the volume integration in (14).

To sum up, the modified PO approach not only outperforms MST in terms of computation times for high frequencies and electrically large canopies, it also enables to account for near-field effects being based on the near-field propagator from [19]. Thus, it supports correct application in rapidly changing environments, which are not known in advance and where the user is often in canopy's near field. As the additional phase shift caused by the canopy is disregarded within the approximation of K in (33), using the full expression for K shall be preferred especially for near-field calculations, as shown in Figs. 4–7.

V. EXPERIMENTAL VALIDATION

In this section, we validate the modified PO model against an experimental data set obtained at 2 GHz for the case of a single isolated tree and we show results obtained by MST as well. For these purposes, a remote controlled airship carrying a Tx instantly pointing toward Rx was utilized. The measurement system transmitted left-handed circularly polarized (LHCP) and right-handed circularly polarized continuous wave signals, which were received by a custom-made sensitive Rx with a high sampling rate of 10 kHz [15]. Here, however, it is sufficient to address only one copolarized channel, namely, LHCP, and, to be consistent with Section IV, vertical polarization will be considered by both the modified PO and MST models. It should be noted that for calibration purposes, measurements on a flat open field were performed to obtain reference LoS signal levels.

For the validation trial, Rx was placed 10 m behind the canopy and the airship made a flyover in the y-direction away from the canopy with a constant speed of about 8 m/s at an altitude of about 200 m. As the Rx antenna height was 1.5 m and the canopy can be modeled by a sphere of 5 m radius with its center 6 m above ground level (see Fig. 8), there exists geometrical LoS up to a horizontal Tx distance of about 150 m from the canopy.

In Fig. 9, we can nicely see that the modified PO model predicts zero attenuation within the geometrical LoS area, as expected, which is also the case of MST. However, the experimental data show excess loss variations of about 2 dB and even signal enhancement of about 3 dB in the LoS region. One reason for this are ground reflections, which were considered neither by the modified PO nor MST and

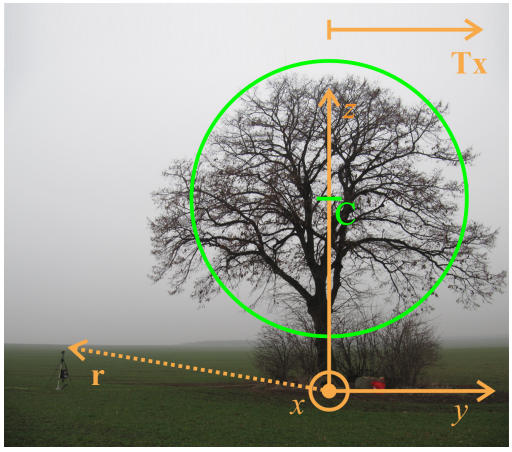

Fig. 8. Single-tree scenario utilized for the experimental validation of the modified PO model and its xyz coordinate system. Rx location is $\mathbf{r} = [0, -10, 1.5]$m, and the canopy can be approximated by a sphere of radius 5 m with its center C $= [0, 0, 6]$m. The airship carrying Tx was moving away from the canopy in the y-direction approximately at a height of 200 m above ground level.

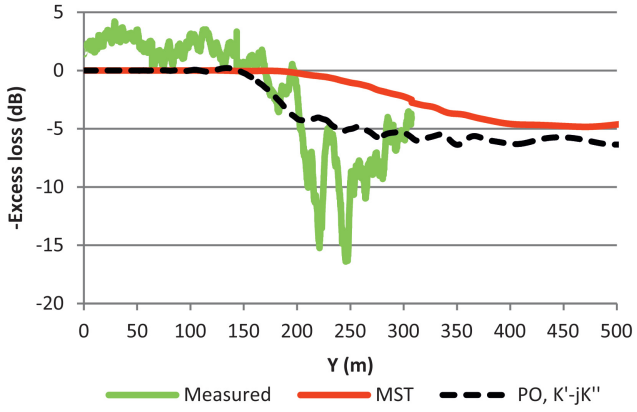

Fig. 9. Experimental validation of the modified PO model against MST and the experimental data obtained at 2 GHz for the single-tree scenario from Fig. 8. Geometrical LoS is achieved approximately up to the horizontal distance of 150 m from the canopy while the forward scatter case is achieved at about 450 m from the canopy where MST and the modified PO model match.

which can, in general, occur between Tx and the canopy, between the canopy and Rx, and between Tx and Rx further shadowed by the tree. In addition, the airship flight path was not perfectly reproduced during the reference open field measurements, and, based on the Rx radiation pattern, the excess loss precision is estimated to be about 1 dB. Also, any reflections from the outer part of the canopy were disregarded in the simulation, which, in reality, contribute to the observed signal variations as well.

When Tx leaves the geometrical LoS region, the measured excess loss increases significantly up to about 10 dB with two deep fades of up to 15 dB. We can see that MST is not capable to reproduce such behavior, mainly because of its far-field approximation as explained in Section IV. Thus, it provides resulting attenuation of about 2 dB only as the forward scatter case was not achieved for any Tx position and only weak coherent scattered fields were obtained. Based on

the geometry, the forward scatter case would be achieved for the y-distance of about 450 m, which is not included in the experimental data but where the simulations in Fig. 9 show a nice match between MST and the modified PO model.

In contrast, the proposed modified PO model provides a smooth and more pronounced transition into the shadowed region, thus matching the experimental data in a significantly better way, respecting both the geometrical LoS borderline and near-field propagation conditions. The predicted attenuation is about 5 dB, which corresponds to the theoretical maximum path of 10 m through the canopy and the specific attenuation of about $\alpha_{\text{spec}} = 0.6$ dB/m calculated by (32) considering a defoliated tree. However, to be consistent with [1]–[3] and [18], the same branches parameters were utilized to obtain this value, which may not be exactly the case of the particular single tree from Fig. 8. By changing these parameters, it would be possible to simply achieve higher specific attenuation and match the excess loss of 10 dB.

As indicated in [2], [3], and [21], the corresponding deep fades are mainly a consequence of ground reflections and individual interactions of the incident field with main branches and trunk, which was not included in the simulation. Despite that, it is obvious that the modified PO model is capable of reproducing both the transition from geometrical LoS to the shadowed area and the resulting attenuation in canopy's near field in a trustworthy way, which is not the case of MST.

VI. Conclusion

We have presented a new model for scattering from tree canopies following a modified PO approach, which enables to account for propagation through the canopy. This is achieved by considering the inner part of the canopy to be illuminated by the incident plane wave, thus acting as an aperture. The incident plane wave is supposed to propagate inside the canopy following the complex propagation constant K, which can be obtained either directly by MST or approximated if the canopy specific attenuation is already known.

The proposed model was tested against MST for the case of artificial single-tree scenarios at 2 and 10 GHz. It was found that when K is not approximated, a better match with MST is achieved for the terrestrial path scenario. The slant path scenario showed that the new model is capable of addressing near-field effects close to the canopy, unlike MST. Furthermore, advantages in the required computation times were demonstrated, especially for the case of high frequencies and electrically large canopies.

In addition, the proposed model was successfully validated against experimental data set at 2 GHz, which include a transition between LoS and shadowed regions. It was shown that a trustworthy match with the experimental data set was achieved with the new model but not with MST.

To sum up, the proposed modified PO/MST model offers a straightforward software implementation built on basis of common PO and enables to avoid MST calculations completely if K is already provided. In addition, it is computation advantageous over MST especially in the case of high frequencies and electrically large structures. Last, but most importantly, it allows for proper near-field calculations within areas close to tree canopies. As such, the model well reproduces both the resulting attenuation by vegetation and transitions between geometrical LoS and shadowed areas behind a canopy.

References

[1] *Attenuation in Vegetation*, document ITU-R Rec. P.833-9, ITU, Geneva, Switzerland, 2016.

[2] Y. L. C. D. Jong and M. H. A. J. Herben, "A tree-scattering model for improved propagation prediction in urban microcells," *IEEE Trans. Veh. Technol.*, vol. 53, no. 2, pp. 503–513, Mar. 2004.

[3] Y. L. C. de Jong, "Measurement and modelling of radiowave propagation in urban microcells," Ph.D. dissertation, Dept. Elect. Eng., Eindhoven Univ. Technol., Eindhoven, The Netherlands, 2001.

[4] A. Ishimaru, *Wave Propagation and Scattering in Random Media*. Hoboken, NJ, USA: Wiley, 1999.

[5] M. A. Karam, A. K. Fung, and Y. M. M. Antar, "Electromagnetic wave scattering from some vegetation samples," *IEEE Trans. Geosci. Remote Sens.*, vol. 26, no. 6, pp. 799–808, Nov. 1988.

[6] L. L. Foldy, "The multiple scattering of waves. I. General theory of isotropic scattering by randomly distributed scatterers," *Phys. Rev.*, vol. 67, nos. 3–4, pp. 107–119, Feb. 1945.

[7] M. Lax, "Multiple scattering of waves," *Rev. Mod. Phys.*, vol. 23, no. 4, pp. 287–310, Oct. 1951.

[8] V. Twersky, "Multiple scattering of electromagnetic waves by arbitrary configurations," *J. Math. Phys.*, vol. 8, no. 3, pp. 589–610, Mar. 1967.

[9] S. A. Torrico, H. L. Bertoni, and R. H. Lang, "Modeling tree effects on path loss in a residential environment," *IEEE Trans. Antennas Propag.*, vol. 46, no. 6, pp. 872–880, Jun. 1998.

[10] K. L. Chee, S. A. Torrico, and T. Kurner, "Radiowave propagation prediction in vegetated residential environments," *IEEE Trans. Veh. Technol.*, vol. 62, no. 2, pp. 486–499, Feb. 2013.

[11] M. Cheffena, F. P. Fontan, F. Lacoste, E. Corbel, H.-J. Mametsa, and G. Carrie, "Land mobile satellite dual polarized MIMO channel along roadside trees: Modeling and performance evaluation," *IEEE Trans. Antennas Propag.*, vol. 60, no. 2, pp. 597–605, Feb. 2012.

[12] F. M. Schubert, M. L. Jakobsen, and B. H. Fleury, "Non-stationary propagation model for scattering volumes with an application to the rural LMS channel," *IEEE Trans. Antennas Propag.*, vol. 61, no. 5, pp. 2817–2828, May 2013.

[13] J. Israel and A. Pajot, "Fading and scattering due to trees in L to Ka band propagation simulations," in *Proc. 9th Eur. Conf. Antennas Propag. (EuCAP)*, Lisbon, Portugal, Apr. 2015, pp. 1–5.

[14] J. Lemorton, X. Boulanger, M. A. Ighil, F. Pérez-Fontán, S. Rougerie, and F. Lacoste, "Mobile and nomadic measurements of the LMS propagation channel at Ku and Ka bands," in *Proc. 9th Eur. Conf. Antennas Propag. (EuCAP)*, Lisbon, Portugal, Apr. 2015, pp. 1–4.

[15] M. Kvicera and P. Pechac, "Seasonal variations of polarization diversity gain in a vegetated area considering high elevation angles and a nomadic user," *Int. J. Antennas Propag.*, vol. 2015, Feb. 2015, Art. no. 194626.

[16] F. Teschl, F. P. Fontan, M. Schonhuber, R. P. Cerdeira, and R. Teschl, "Attenuation of spruce, pine, and deciduous woodland at C-band," *IEEE Antennas Wireless Propag. Lett.*, vol. 11, pp. 109–112, 2012.

[17] P. Horak and P. Pechac, "Excess loss for high elevation angle links shadowed by a single tree: Measurements and modeling," *IEEE Trans. Antennas Propag.*, vol. 60, no. 7, pp. 3541–3545, Jul. 2012.

[18] M. Kvicera, J. Israel, F. Pérez-Fontán, and P. Pechac, "Sensitivity analysis of multiple scattering theory applied to tree canopies at microwave frequencies," *IEEE Antennas Wireless Propag. Lett.*, vol. 15, pp. 1175–1178, Nov. 2015.

[19] L. Diaz and T. Milligan, *Antenna Engineering Using Physical Optics: Practical CAD Techniques and Software*, Norwood, MA, USA: Artech House, 1996.

[20] C. A. Balanis, *Advanced Engineering Electromagnetics*. Hoboken, NJ, USA: Wiley, 2012.

[21] M. Kvicera, F. Pérez-Fontán, and P. Pechac, "Scattering from single isolated tree based on physical optics: Preliminary model," in *Proc. 9th Eur. Conf. Antennas Propag. (EuCAP)*, Lisbon, Portugal, Apr. 2015, pp. 1–4.

[22] S. A. Torrico and R. H. Lang, "A simplified analytical model to predict the specific attenuation of a tree canopy," *IEEE Trans. Veh. Technol.*, vol. 56, no. 2, pp. 696–703, Mar. 2007.